THE JOURNAL OF BIOLOGICAL CHEMISTRY VOL. 287, NO. 4, pp. 2398–2409, January 20, 2012

Characterization of Heparin-induced Glyceraldehyde-3-phosphate Dehydrogenase Early Amyloid-like Oligomers and Their Implication in α-Synuclein Aggregation*[S]

Received for publication, September 12, 2011, and in revised form, November 21, 2011 Published, JBC Papers in Press, December 1, 2011, DOI 10.1074/jbc.M111.303503

Clarisa M. Torres-Bugeau[‡1], César L. Ávila[‡2], Rita Raisman-Vozari[§], Dulce Papy-Garcia[¶], Rosangela Itri[‖3], Leandro R. S. Barbosa[‖], Leonardo M. Cortez[**], Valerie L. Sim[**], and Rosana N. Chehín[‡2,4]

*From the [‡]Instituto Superior de Investigaciones Biológicas, CCT-Tucumán and Insitituto de Química Biológica Dr Bernabé Bloj (CONICET-UNT), Tucumán T4000ILI, Argentina, [§]INSERM, UMRS 975, CRICM, ICM, Thérapeutique Expérimentale de la Neurodégénérescence, Paris 91010 Créteil Cedex, France, the [¶]Laboratoire CRRET EAC CNRS 7149, Université Paris Est Créteil, 94010 Créteil, France, the [‖]Instituto de Física da Universidade de São Paulo, São Paulo 05508-900, Brazil, and the **Centre for Prions and Protein Folding Diseases, University of Alberta, Edmonton, Alberta T6G 2M8, Canada*

Background: GAPDH and glycosaminoglycans (GAGs) have been routinely found in Parkinson disease amyloid aggregates.
Results: Heparin and heparan sulfate induce the formation of GAPDH amyloid-like oligomers, which were characterized by using biophysical techniques.
Conclusion: Heparin-induced GAPDH early oligomeric species are able to reduce the amount of α-synuclein (AS) prefibrillar species.
Significance: GAPDH oligomeric species might be taken into account in recruiting of AS toxic species.

Lewy bodies and Lewy neurites, neuropathological hallmarks of several neurological diseases, are mainly made of filamentous assemblies of α-synuclein. However, other macromolecules including Tau, ubiquitin, glyceraldehyde-3-phosphate dehydrogenase, and glycosaminoglycans are routinely found associated with these amyloid deposits. Glyceraldehyde-3-phosphate dehydrogenase is a glycolytic enzyme that can form fibrillar aggregates in the presence of acidic membranes, but its role in Parkinson disease is still unknown. In this work, the ability of heparin to trigger the amyloid aggregation of this protein at physiological conditions of pH and temperature is demonstrated by infrared and fluorescence spectroscopy, dynamic light scattering, small angle x-ray scattering, circular dichroism, and fluorescence microscopy. Aggregation proceeds through the formation of short rod-like oligomers, which elongates in one dimension. Heparan sulfate was also capable of inducing glyceraldehyde-3-phosphate dehydrogenase aggregation, but chondroitin sulfates A, B, and C together with dextran sulfate had a negligible effect. Aided with molecular docking simulations, a putative binding site on the protein is proposed providing a rational explanation for the structural specificity of heparin and heparan sulfate. Finally, it is demonstrated that *in vitro* the early oligomers present in the glyceraldehyde-3-phosphate dehydrogenase fibrillation pathway promote α-synuclein aggregation. Taking into account the toxicity of α-synuclein prefibrillar species, the heparin-induced glyceraldehyde-3-phosphate dehydrogenase early oligomers might come in useful as a novel therapeutic strategy in Parkinson disease and other synucleinopathies.

Parkinson disease (PD)[5] is the second most common neurodegenerative disorder with motor alterations resulting from the loss of dopaminergic neurons in the *substantia nigra.* Histopathologically, PD and related disorders called synucleinopathies (1) are characterized by the presence of intraneuronal inclusions (Lewy bodies, LB) and dystrophic neurites (Lewy neurites) (2, 3). It is generally accepted that the fibrillar aggregation of α-synuclein (AS) is a critical factor in the etiology of PD because LB and Lewy neurites contain as a main component a misfolded, fibrillar, and phosphorylated form of this protein (4, 5). However, other macromolecules as GAPDH (6), ubiquitin (7), and glycosaminoglycans (GAGs) (8) are routinely found associated with amyloid deposits in most amyloidosis diseases (9, 10). In addition, evidence from *in vitro* studies support an active role of GAGs in amyloid fibril formation (11–14). Even though there is strong experimental evidence implicating GAGs in the amyloidogenic process, the molecular mechanism by which GAGs promote the amyloid formation remains obscure as well as the ability of GAGs to interact with other LB components like GAPDH.

GAPDH is a ubiquitously expressed enzyme largely known for its glycolytic activity, but nowadays it is considered as a moonlighting protein because it plays individual functions

* This work was supported by Consejo Nacional de Investigaciones Cientificas y Tecnicas (CONICET) Grants PIP 2518 and Consejo Investigaciones de la Universidad Nacional de Tucuman (CIUNT) Grant 26/D439-1.
[S] This article contains supplemental Table S1 and Figs. S1 and S2.
[1] Recipient of a CONICET fellowship.
[2] Researcher of CONICET.
[3] Recipient of a Conselho Nacional de Desenvolvimento Científico e Tecnológico (CNPq) research fellowship.
[4] To whom correspondence should be addressed: INSIBIO, Chacabuco 461 (4000)-Tucuman-Argentina. Tel./Fax: 54-381-4248921; E-mail: rosana@fbqf.unt.edu.ar.

[5] The abbreviations used are: PD, Parkinson disease; LB, Lewy body(ies); AS, α-synuclein; GAG, glycosaminoglycan; HS, heparan sulfate; ThT, thioflavin T; CS, chondroitin sulfate; Dx, dextran; G3P, glycerol-3-phosphate; ANS, 1-anilinonaphthalene-8-sulfonic acid; SAXS, small angle x-ray scattering; DLS, dynamic light scattering; FTIR, Fourier transformed Infrared.

depending on its cellular locations and oligomeric state (15–17). In fact, GAPDH is involved in apoptosis, neuronal disorders, viral pathogenesis, endocytosis, microtubule bundling, phosphotransferase/kinase reactions, translational regulation of gene expression, nuclear RNA export, DNA replication, and DNA repair (17). In the extracellular space, GAPDH has an immunoglobulin production-stimulating factor activity (18), as well as a cell-cell and/or cell-matrix interaction modulating activity, as an anti-adhesive factor (19). GAPDH was also involved in both the etiology and as a target in the treatment of PD (20). It has been recently shown that the overexpression of both GAPDH and AS in COS-7 cells induced LB-like cytoplasmic inclusions. In fact, it has been suggested that AS itself is not sufficient to cause aggregation into LB-like inclusions (21). Also, drugs currently used to treat PD bind to or affect GAPDH functions (22, 23).

At physiological conditions of pH and temperature, GAPDH remains in its homotetrameric globular soluble state. However, in the presence of acidic membranes, GAPDH forms amyloid fibrils (24) via a nucleation-dependent mechanism involving an unexpected short nucleation lag time (25). Moreover, the GAPDH aggregates formed under these conditions appear to be similar to disease-related amyloid fibrils, suggesting that this process could also be involved in amyloid formation *in vivo* (24).

Results in the present paper demonstrate that heparin and heparan sulfate (HS) promotes the GAPDH fibrillar aggregation at physiological conditions of pH and temperature through the formation of amyloid-like oligomers. In addition, the ability of these early oligomeric species to modulate AS aggregation kinetics is also demonstrated. The results presented herein could justify of the presence of GAGs and GAPDH in LB, raising a new hypothesis where the aggregation process might be multi-component and that GAGs may first participate in the formation of GAPDH oligomers, which will further act as catalysts on the fibrillation processes of other proteins.

EXPERIMENTAL PROCEDURES

Materials—GAPDH (EC 1.2.1.12), thioflavin T (ThT), high molecular weight heparin sodium salt, HS, chondroitin sulfate (CS)-A, CS-B, CS-C, and Tris (2,2-bipyridyl)dichlororuthenium(II) hexahydrate (RuBpy) were from Sigma-Aldrich. Dextran (Dx) was from Amersham Biosciences. The GAPDH solutions were prepared in a 20 mM HEPES buffer, pH 7.4. Polysaccharides heparin and HS were dissolved in the prefiltered HEPES buffer. Expression and purification of human AS were performed as previously described (26). The purity of the protein was assessed by SDS-PAGE. Monomeric AS stock solutions were prepared in 20 mM HEPES, pH 7.4. Prior to measurements, protein solutions were filtered and centrifuged for 30 min at 12,000 × *g*. The protein concentration was determined by the measurement of absorbance at 280 nm using extinction coefficient $\epsilon_{280} = 1.17 \times 10^5\ cm^{-1}\ M^{-1}$ (27) and $\epsilon_{280} = 5600\ cm^{-1}\ M^{-1}$ for GAPDH and AS (26), respectively.

Aggregation Kinetics Measured by Thioflavin T Fluorescences—A 2.5 mM ThT solution was prepared in a 20 mM HEPES buffer, pH 7.4. In a thermostatted spectrofluorometer cuvette, 75 μg/ml of heparin, CS-A, CS-B, CS-C, Dx, or HS were added to a final 0.16 mg/ml of protein solution, and after the addition of 25 μM ThT, each mixture was measured with a ISS (Champaign, IL) PC1 spectrofluorometer according to LeVine (28). To test the influence of glycerol-3-phosphate (G3P) in the heparin-induced GAPDH aggregation kinetics, 0.16 mg/ml of GAPDH was preincubated with 1 mM of G3P for 5 min with different heparin concentrations: 75, 150, 300, and 600 μg/ml. A background fluorescence spectrum obtained by running a blank buffer was subtracted from each sample fluorescence spectrum. The excitation wavelength was set at 450 nm, and the emission was measured at 482 nm using slit widths of 0.5 and 1 nm for excitation and emission light paths, respectively. Fluorescence intensity at 482 nm was analyzed along the time, and the kinetic profile data were fitted to an exponential function $I_t = I_\infty(1 - e^{-t/\tau})$, where τ is the time (t) at which the fluorescence intensity (I_t) reaches 63.2% of the maximal value (I_∞). Each curve represents the average of at least three independent experiments.

Fluorescence Microscopy—4 mg/ml of GAPDH were incubated in the presence of 1.9 mg/ml of heparin at 37 °C with orbital agitation. Aliquots withdrawn at 0, 1, 5, and 24 h were centrifuged 30 min at 12,000 × *g*. The pellets was resuspended and incubated with 0.2 mg/ml thioflavin S for 90 min at room temperature under stirring. Then fibrils were washed by centrifugation and resuspension in freshly prepared buffer three times to remove excess of thioflavin S. The obtained fibrils were finally resuspended in buffer HEPES, pH 7.4, to be observed under BX51 microscopy OLYMPUS (Japan).

Tryptophan Intrinsic Fluorescence Studies—The mixture GAPDH:heparin was incubated under agitation for 24 h at 37 °C, pH 7.4, at a final concentration of 0.16 mg/ml and 75 μg/ml, respectively. Fluorescence spectra was collected using $\lambda_{ex} = 295$ nm and λ_{em} in the range 310–400 nm, known to be specific for tryptophan. The wavelength shift was monitored using the integral midpoint of the curve. The slit widths were set to 1 nm.

ANS Fluorescence Assay—Aliquots from the incubated GAPDH:heparin mixture were taken at different times and treated with 5 μM 1-anilinonaphthalene-8-sulfonic acid (ANS) in 20 mM HEPES buffer, pH 7.4. The excitation wavelength was 350 nm, and fluorescence emission spectra were collected between 400 and 600 nm. The values of fluorescence intensity and the values of maximal wavelength of the emission spectra were plotted against time.

Infrared Spectroscopy Measurements—Samples at 4 mg/ml of GAPDH for FTIR spectroscopy either in the presence or in the absence of 1.9 mg/ml GAGs were prepared by dissolving the lyophilized protein in a 20 mM pD 7 D_2O-HEPES buffer. The samples were assembled in a thermostatted cell between two CaF_2 windows with a pathlength of 100 μm. A tungsten-copper thermocouple was placed directly onto the window, and the temperature was controlled all over the measurements. The spectra were recorded in a Nicolet 5700 spectrometer equipped with a DTGS detector (Thermo Nicolet, Madison, WI). The sample chamber was permanently purged with dry air. The spectra were generated by averaging 128 interferograms collected with a nominal resolution of 2 cm^{-1} and apodized with a Happ-Genzel function. The D_2O contribution in the amide I′ region was eliminated by subtracting the buffer spectra from

that of the solution at the same temperature to obtain a flat baseline between 2000 and 1700 cm^{-1}. Determination of peak position and curve fitting were performed as reported previously (29, 30). Briefly, band component positions were obtained from deconvolution and derivation. Because the results obtained after iterations may not be unique, the following restrictions were applied: (i) from initial guesses, the band position could not diverge more than the distance between data points, and (ii) the width of the bands should be less than one-half of the amide I′ bandwidth. The use of several spectra recorded at different incubation times reduces the error of the quantification procedure to ~3% (31). The band assignment was performed according to Cortez *et al.* (25), which is in good agreement with x-ray data (32). The error in determination of the FTIR structural analysis from the amide I′ band from different runs is ~2%. Protein structural analyses, either in the absence or in the presence of the GAGs, were repeated three times with fresh new samples to test the reproducibility of the measurements.

Circular Dichroism Measurement—Samples at 4 mg/ml of GAPDH in 20 mM HEPES, pH 7.4, were incubated in test tube at 37 °C either in the presence or in the absence of 1.9 mg/ml heparin. At indicated time points, aliquots were removed for CD measurements. Circular dichroism spectra were recorded on an Applied Photophysics Chirascan (UK) instrument. A cell with a 0.1-mm pathlength was used for spectra recorded between 190 and 260 nm, with sampling points every 1 nm. For each sample, 10 scans were averaged, and baseline spectra were subtracted. The data were processed using Applied Photophysics Chirascan Viewer and Microsoft Excel.

Small Angle X-ray Scattering (SAXS) Measurements—The SAXS experiments were performed at the National Synchrotron Light Laboratory (Campinas, Brazil) at 37 °C, with radiation wavelength $\lambda = 1.488$ Å and sample-to-detector distance of ~1000 mm, which enabled collection of the following scattering vector interval from $q_{min} = 0.02$ $Å^{-1}$ to $q_{max} = 0.32$ $Å^{-1}$,

$$q = \frac{4\pi}{\lambda}\sin(\theta) \qquad \text{(Eq. 1)}$$

where being 2θ the scattering angle. The q_{min} value allowed us to determine the scattering particles maximum dimension, D_{max}, of ~300 Å ($D_{max} = 2\pi/q_{min}$, according to the sampling theorem (33). The samples were set between two mica windows and a 1-mm spacer, handled in a liquid sample holder. This was placed perpendicular to the primary x-ray beam. The obtained curves collected every 2 min were corrected for detector homogeneity (bi-dimensional position-sensitive detector) and normalized by taking into account the decrease of the x-ray beam intensity during the experiment. The parasitic background from the buffer solution was subtracted, considering the sample's attenuation. Solutions of 4 mg/ml of GAPDH were prepared in 20 mM HEPES buffer at pH 7.4 in the absence and in the presence of heparin at 1.9 mg/ml.

SAXS Theory—The SAXS intensity, $I(q)$, of an isotropic solution of noninteracting scattering particles can be described as follows,

$$I(q) = kn_pP(q) \qquad \text{(Eq. 2)}$$

where n_p corresponds to the particle number density, and k is a normalization factor related to the instrumental effects (33, 34). $P(q)$ is the orientational average of the particle form factor and gives information on the scattering particle size and shape. For proteins with known crystallographic structure, $P(q)$ can be modeled from the atomic coordinates of its crystallographic structure deposited in the Protein Data Bank. In the present work, SASMOL software (34, 35) and the Protein Data Bank entry 1J0X were used to calculate $P(q)$ corresponding to the homotetramer GAPDH structure.

To study how heparin impacts on GAPDH conformation along the time, we investigated the evolution of the protein radius of gyration, R_g, and the distance distribution function, $p(r)$, as follows. It is well known that $I(q)$ can be described at low q values (36),

$$I(q \to 0) \cong I(0)e^{\frac{R_g^2 q^2}{3}} \qquad \text{(Eq. 3)}$$

which is known as Guinier's law. So, a simple plot of $Ln\, I(q) \times q^2$ gives information of the protein radius of gyration, R_g. Moreover, a Fourier transform connects $P(q)$, and hence $I(q)$, to the pair distance distribution function, $p(r)$ (33, 36). Such a function is model-free and represents the probability of finding a pair of small elements, at a distance r, within the entire volume of the scattering particle, providing information about the scattering particle shape and its R_g. The scattering particle maximum dimension, D_{max}, is accounted for by a certain r value where $p(r)$ goes to 0. In the case of globular macromolecules, $p(r)$ is symmetric and has a maximum frequency of distances of approximately $D_{max}/2$. For elongated macromolecules, $p(r)$ assumes an anisometric distribution of distances. In the current work, GNOM software is used (37) to calculate the $p(r)$ functions from the experimental scattering curves.

Dynamic Light Scattering (DLS) Measurements—DLS measurements were performed in a Brookhaven Instruments apparatus, which consists of a HeNe (632 nm and 35 milliwatt) laser coupled to a BI-200SM goniometer with a digital autocorrelator BI-9000AT. Samples placed into cylindrical glass tubes (13 × 100 mm) were maintained at a fix temperature of 37.0 ± 0.1 °C controlled by a water circulatory system. DLS was used to follow changes of GAPDH hydrodynamic diameter under the influence of heparin along the time. The samples consisted of 1.5 ml of a 4 mg/ml GAPDH solution in the absence and in the presence of 1.9 mg/ml heparin. Measurements were made at an angle $\theta = 90°$ to the incident beam, and the data were collected at every 60 s. The first data acquirement was performed 250 s after heparin in addition to a GAPDH solution to ensure the homogeneity of the sample. The correlation functions were analyzed to obtain the distributions of the decay rates and, hence, the apparent diffusion coefficients and ultimately the distributions of the hydrodynamic radius of the scattering particles in solution via Stokes-Einstein equation (38).

GAPDH Enzymatic Activity Assay—The enzymatic reaction was followed in a reaction mixture containing 100 mM glycine, 100 mM Na_2HPO_4, 5 mM EDTA, 1.5 mM NAD^+, and 2 mM G3P at 25 °C, pH 9.0. 0.16 mg/ml of GAPDH was incubated in the presence or in the absence of 75 μg/ml of heparin at 37 °C, pH 7.4. Fractions of 20 μl were taken at each time and were added

to the above-mentioned mixture. The enzymatic activity was measured following the increase in the absorbance of NADH at 340 nm using a Beckman DU-7500 spectrophotometer (39).

Docking Calculation—A global search for heparin-binding sites on GAPDH was conducted using the program AutoDock (version 4.2). The crystal structure for rabbit muscle GAPDH was taken from the Protein Data Bank (entry 1J0X) (32). In addition, the structures of several protein-heparin complexes, such as acidic fibroblast growth factor, basic fibroblast growth factor, and hepatocite growth factor (referred herein as the test set), were used to evaluate the prediction capability of the docking protocol. The Autodock Tools package was used for setting up all input files for docking calculations. An ensemble of initial structures for the ligand probes was prepared from the test set. Partial charges for the probe atoms were adapted from Bitomsky and Wade (40). Grids of probe atom interaction energies were computed with a spacing of 0.5 Å spanning the entire proteins solvent accessible surfaces. A total of 3000 hard-docked configurations (1000 for each conformation of the ligand with all rotable bonds fixed) were generated using a Lamarckian genetic algorithm and clustered with a 2.0 Å threshold. A focused docking experiment using a grid spacing of 0.375 Å and a semi-rigid ligand was derived from 256 different runs around the sites with lowest interaction energy from the previous step. The lowest energy structure from the largest cluster was considered as the best docking solution.

The figures were composed using VMD (41). Electrostatic potentials for GAPDH were computed using APBS (42). The schematic diagrams for the interactions between the docked hexasaccharide and the protein were generated with LIGPLOT (43).

Preparation of GAPDH Fibrils—GAPDH fibril preparation was performed in 4 mg/ml GAPDH solutions as follows. Two ml of freshly prepared protein solution was incubated at 37 °C under constant orbital agitation in the presence of 1.9 mg/ml of heparin. The fibril formation was followed by ThT binding and infrared spectroscopy, using aliquots withdrawn during the time. After 24 h of incubation, the formed fibrils were washed by centrifugation to remove heparin and soluble protein. The amount of protein was estimated according to Lowry *et al.* (44), and heparin was estimated according to Dische *et al.* (45).

Cross-seeding Experiments—70 μM of AS solution was incubated under orbital agitation at 37 °C during 48 h either alone, with 18.5 μg/ml of heparin, 50 μM of GAPDH, or 0.3 and 50 μM of GAPDH taken from the incubation mixture at different times corresponding to oligomers (5, 15, 30, and 60 min) and fibrils (24 h). The reaction was followed by ThT fluorescence using aliquots withdrawn during the time.

Gel Electrophoresis in SDS-PAGE under Denaturing Conditions—500 μl of freshly prepared GAPDH:heparin mixture was preincubated at 37 °C under agitation for 15 min and then added to 70 μM of AS for a final volume of 2 ml. The reaction mixture was incubated 5 h at 37 °C with agitation, and then it was washed twice by centrifugation at 12000 g during 30 min. The fibrils were resuspended in 8 M of urea, mixed with SDS loading buffer, and boiled for 10 min. 15 μl of each sample was loaded per lane on SDS gels. Electrophoresis was carried out in a Bio-Rad Mini PROTEAN® system in slab gels using the buffer and fixing described by Weber and Osborn (46) in 12% acrylamide gel. The gel was stained with the Coomassie Blue staining method. The protein molecular weight markers were Precision Plus Protein™ standards (Bio-Rad).

RESULTS

Fluorescence Studies of Heparin-induced GAPDH Aggregation—The ability of heparin to induce GAPDH aggregation was monitored by ThT binding assay (28). In the absence of heparin, no aggregation of GAPDH was detected, even after 24 h of incubation at 37 °C, suggesting that the enzyme remains in its soluble state. Heparin efficiently induced an increase in ThT fluorescence emission, and the process could be fitted to a single exponential kinetics with a time constant (τ) of 12.5 $\pm$ 2.0 min (Fig. 1*A*). However, the presence of amyloid fibrils could be detected by thioflavin S fluorescence microscopy only after 5 h of incubation (Fig. 1*B*). A decay of protein concentration in the supernatant of extensively centrifuged samples is only evident after 4 h of incubation, which is also in accordance with the absence of protein fibrils during the early stages of the process. Taken together, these results suggest that the increment in ThT fluorescence observed can be attributed to the presence of GAPDH soluble oligomers as seen on other systems (47, 48).

ANS was also used to test for heparin-induced GAPDH conformational changes. The fluorescent intensity of this dye is greatly enhanced on binding to hydrophobic surfaces accompanied by a blue shift in its fluorescence maximum from ~515 to ~475 nm. In the presence of GAPDH, the emission intensity of ANS shows a peak (λ_{max}) centered at 524 nm, characteristic of the free dye. A significant blue shift toward 450 nm is observed 5 min after the addition of heparin, accompanied by a small increase in the fluorescence intensity (Fig. 1*C*). The value of λ_{max} reaches 425 nm with an increase in the fluorescence of ~20% upon 1 h of heparin-GAPDH interaction (Fig. 1*C*). These changes indicate the appearance of new solvent-exposed hydrophobic regions. A final shift in fluorescence emission toward 412 nm was observed after 5.0 h of incubation, which might be indicative of further structural changes in GAPDH.

Changes in the environment and solvent accessibility of Trp residues in GAPDH during the aggregation process were monitored through intrinsic fluorescence emission over time. In the absence of heparin, GAPDH showed a broad peak centered at 339 nm arising from Trp^{84}, Trp^{193}, and Trp^{310}. It is important to note that two of the Trp residues (Trp^{193} and Trp^{310}) are located at the interface between subunits, whereas Trp^{84} is deeply buried in the structure of the native GAPDH tetramer according to the crystallographic structure (32) (supplemental Table S1 and Fig. S1). A red shift of 3 nm was promptly observed in the first 5 min of heparin contact to the protein (Fig. 1*D*), which may be an indicative of some solvent exposure of at least one of the Trps. Note that such red shift evolves to 344–345 nm after 1–6 h of heparin addition, reaching a value of 350 nm after 24 h (Fig. 1*D*).

To characterize the early GAPDH oligomers, in the following sections the time scale was focused in the first hour of incubation where soluble oligomeric species are present. The total ThT signal showed a dose-dependent increase with heparin concentrations in a range between 25 and 150 μg/ml (Fig. 2*A*, *closed bars*). However, no changes in the rate of

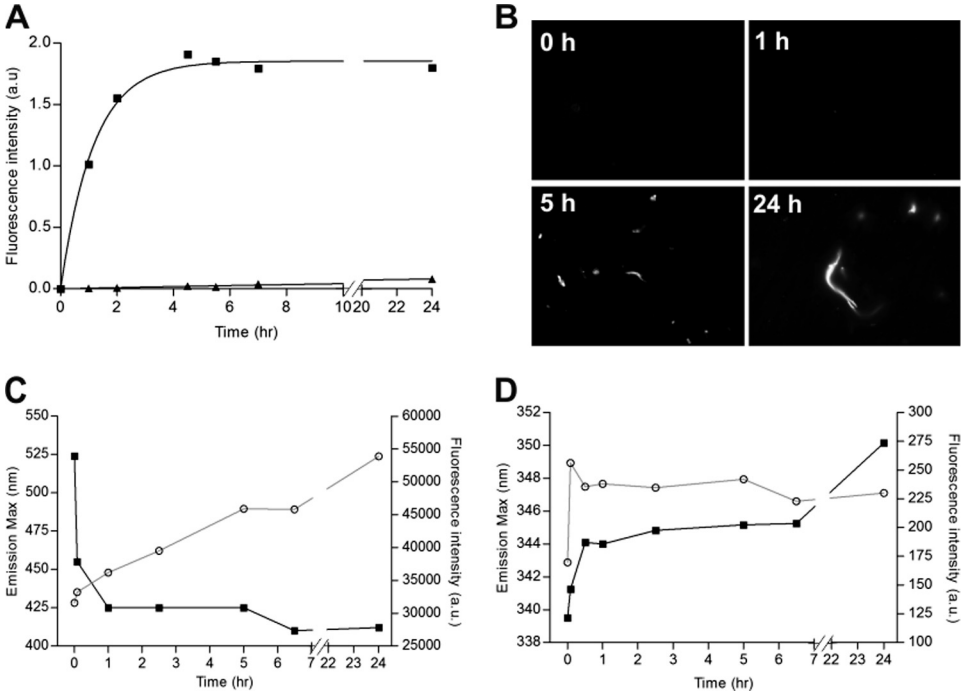

FIGURE 1. **Effect of heparin on GAPDH fibrillation kinetic study by fluorescence techniques.** *A*, GAPDH aggregation kinetics measured by thioflavin T fluorescence emission. GAPDH alone (▲) or in the presence of 75 μg/ml of heparin (■). *B*, thioflavin S fluorescence microscopy of GAPDH-heparin interaction at 0, 1, 5, and 24 h. Final protein concentration was 4 mg/ml and magnification 100×. *C* and *D*, changes in ANS (*C*) and Trp (*D*) fluorescence emission spectra corresponding to the fluorescence intensity (○) at the peak of the emission wavelength (■).

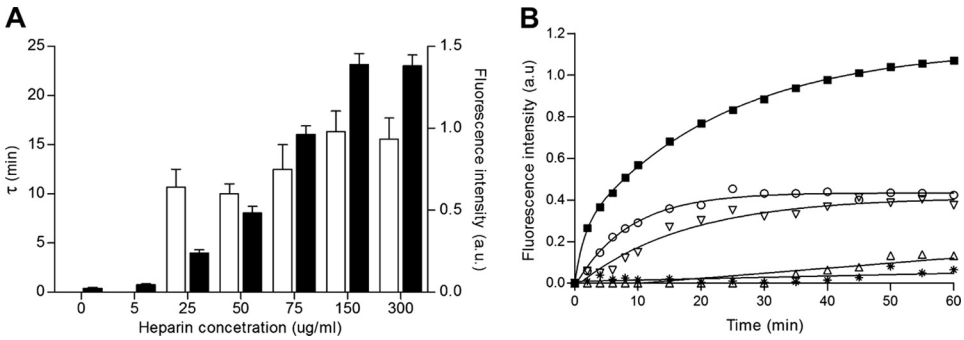

FIGURE 2. *A*, heparin dose dependence of GAPDH aggregation: characteristic time τ (*open bars*) and final amount (*closed bars*) of ThT fluorescence after 1 h of incubation at 37 °C of GAPDH (0. 16 mg/ml) in the presence of increasing amount of heparin. *B*, effect of G3P (1 mM) on heparin-induced GAPDH aggregation measured in the presence of different heparin concentrations: 75 μg/ml (*), 150 μg/ml (△), 300 μg/ml (▽), and 600 μg/ml (○). The GAPDH (0.16 mg/ml) aggregation kinetics induced by 75 μg/ml of heparin in the absence of G3P is also represented (■). The *line* represents the curve fit according to the equation described under "Experimental Procedures."

oligomer formation were observed varying the heparin concentration (Fig. 2*A*, *open bars*). This suggests that the GAPDH:heparin binding is not rate-limiting in the formation of oligomeric species.

In the presence of 1 mM G3P, heparin was unable to induce GAPDH aggregation (Fig. 2*B*). The G3P binding site is made of residues from the four subunits (49), and therefore the enzyme tetrameric form is stabilized by the presence of its natural substrate. Fig. 2*B* also shows that increasing the heparin concentration, the substrate inhibition could be partially reverted, suggesting a competition between G3P and heparin for the enzyme binding.

FTIR Characterization of Heparin-induced GAPDH Oligomers—Heparin-induced GAPDH tertiary and/or quaternary structural changes were studied by infrared spectroscopy as a function of time (Fig. 3*A*). As was previously described, the GAPDH spectrum is characterized by two dominant bands at 1653 and 1637 cm^{-1} that reflect the α-helix and β-sheet content, respectively (Fig. 3*B*). Other bands appearing at ~1642 cm^{-1} were assigned to nonstructured conformations, the band at 1623 cm^{-1} corresponds to the tetramer interoligomeric contact, whereas the band near 1667 cm^{-1} arise from β-turns, and the band at 1680 cm^{-1} may also arise from a small contribution of the high frequency vibration of the anti-parallel β-strand (25). The GAPDH spectrum remained unchanged after 24 h of incubation at 37 °C (not shown). However, after heparin addition, significant changes in the shape of the amide I′ band became evident during the incubation time. The contribution from a band attributable to cross-β structure (located near 1616 cm^{-1}) increased significantly during the incubation time (Fig. 3, *C–E*).

To further characterize the changes in the amide I′ band, deconvolution, and curve fitting procedures were performed.

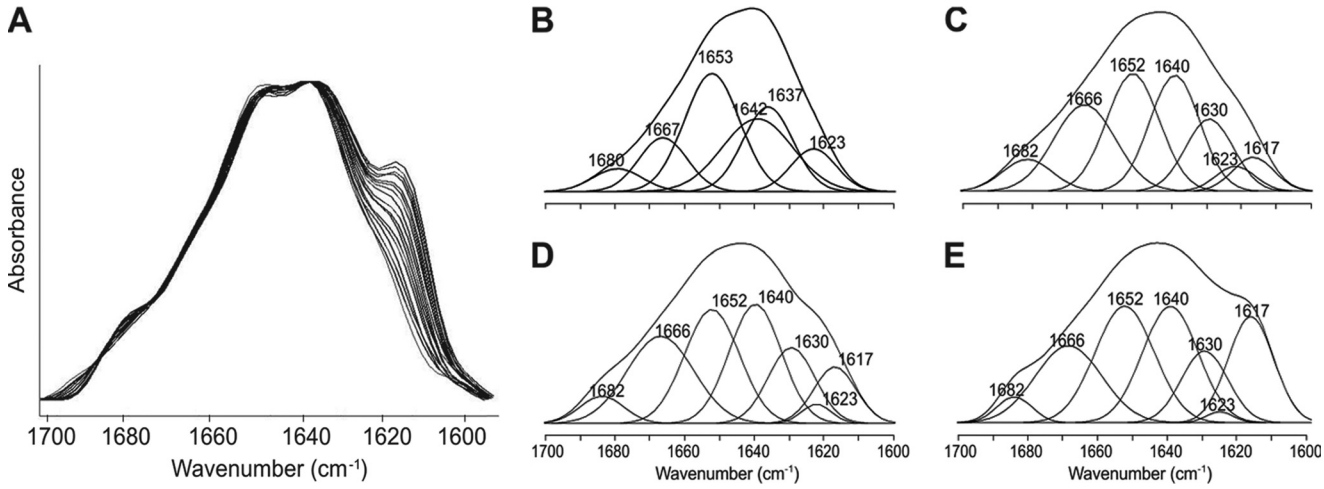

FIGURE 3. **Heparin-induced GAPDH conformational changes measured by infrared spectroscopy.** *A*, time evolution of the FTIR spectra of the deconvoluted amide I′ region of GAPDH (4 mg/ml) during oligomer formation at 37 °C and pD 7. The samples were collected after 1.9 mg/ml of heparin addition in different periods of time, every 3 min until the first 60 min were reached. *B–E*, analysis of GAPDH amide I′ band after the curve fitting procedure (see "Experimental Procedures") showing the component bands: GAPDH alone (*B*) and after 5 min (*C*), 1 h (*D*), and 24 h (*E*) of heparin addition.

TABLE 1

Band position and percentage area corresponding to the components obtained after curve fitting of the GAPDH amide I′ band in the absence or in the presence of heparin at different incubation times

Position	Area
	%
GAPDH	
1616 cm^{-1}	<1
1623 cm^{-1}	11
1637 cm^{-1}	21
1642 cm^{-1}	19
1653 cm^{-1}	29
1667 cm^{-1}	13
1680 cm^{-1}	7
GAPDH:heparin (1 h)	
1618 cm^{-1}	6
1623 cm^{-1}	4
1630 cm^{-1}	16
1640 cm^{-1}	22
1652 cm^{-1}	25
1666 cm^{-1}	21
1682 cm^{-1}	6
GAPDH:heparin (24 h)	
1616 cm^{-1}	17
1623 cm^{-1}	1
1630 cm^{-1}	13
1640 cm^{-1}	21
1652 cm^{-1}	26
1665 cm^{-1}	19
1682 cm^{-1}	3

The relative contribution of different structural elements to the amide I′ is summarized in Table 1. The 1623 cm^{-1} band, which was previously attributed to the contacts between subunits (25), diminished after 1 h of incubation. It is important to note the downshift of band attributable to β-sheet to lower wavelengths (from 1637 to 1630 cm^{-1}) in a context where the overall β-sheet content remains almost constant indicative of a shortening in intramolecular hydrogen bonds of the β-sheets located at the edge of the monomers (β-edge) (50). These results suggest that heparin-induced GAPDH early oligomers have an overall amyloid-like conformation with an incremented amount of cross-β structure. After 24 h of incubation, when fibrils became detectable by microscopy (Fig. 1*B*), an increment in the bands attributable to cross-β structure and β-turns was observed (Table 1).

SAXS Characterization of Heparin-induced GAPDH Oligomers—To characterize the size and shape of the heparin-induced GAPDH oligomers, SAXS studies were performed. Under the experimental condition used in this work, SAXS curves for GAPDH in solution were in good agreement with those derived from the theoretical homotetrameric model of the protein crystallographic structure (Protein Data Bank entry 1J0X) with a R_g of 32.9 Å (Fig. 4*A*). The possibility of protein dissociation and oligomerization at 37 °C was checked. No changes in the SAXS curves were observed for up to 1 h of consecutive data acquisition from GADPH scattering, revealing the high protein stability in our experimental conditions. The corresponding $p(r)$ curve is presented in Fig. 4*C*. Note that the $p(r)$ function from the homotetramer structure (*solid line*) can nearly superpose to the experimental one, evidencing that the protein did not suffer any change in the absence of heparin at physiological temperature. Moreover, $p(r)$ is centered at $r = 40$ Å, corresponding to the maximum frequency of distances inside the protein, which has a maximum dimension D_{max} of ~87 Å. In contrast, after heparin addition, we observe an increasing upturn in the scattering intensity at low q values (Fig. 4*B*) that indicates the formation of larger aggregates in solution (51). Concomitantly, we also note a smoothness of the shoulder at $q = 0.15$ $Å^{-1}$ characteristic of the homotetramer structure (Fig. 4*A*). The analysis of the radius of gyration R_g (Fig. 4*B*, *inset*) revealed that R_g changed from 32 ± 2 Å, in the absence of heparin, to 50 ± 1 Å and to ~66 ± 1 Å after 2 and 60 min of protein-heparin interaction, respectively. Interestingly, $p(r)$ functions (Fig. 4*C*) evidence that heparin promoted some changes in the homotetramer structure already at 2 min of GAPDH-heparin interaction, because the maximum of frequencies was displaced to $r = \sim 50$ Å and D_{max} was enlarged to 190 Å. Such a result is compatible to a small change in the protein conformation, probably because of a small opening of the structure induced by heparin binding. This would lead to an increment in the distance r between scattering centers inside GAPDH with the maximum frequency of occurrence displaced from 40 to 50 Å. Further, the increase in protein maximum distance D_{max} to 190 Å in the $p(r)$ function (Fig. 4*C*) and in R_g to 50 Å, both related to the

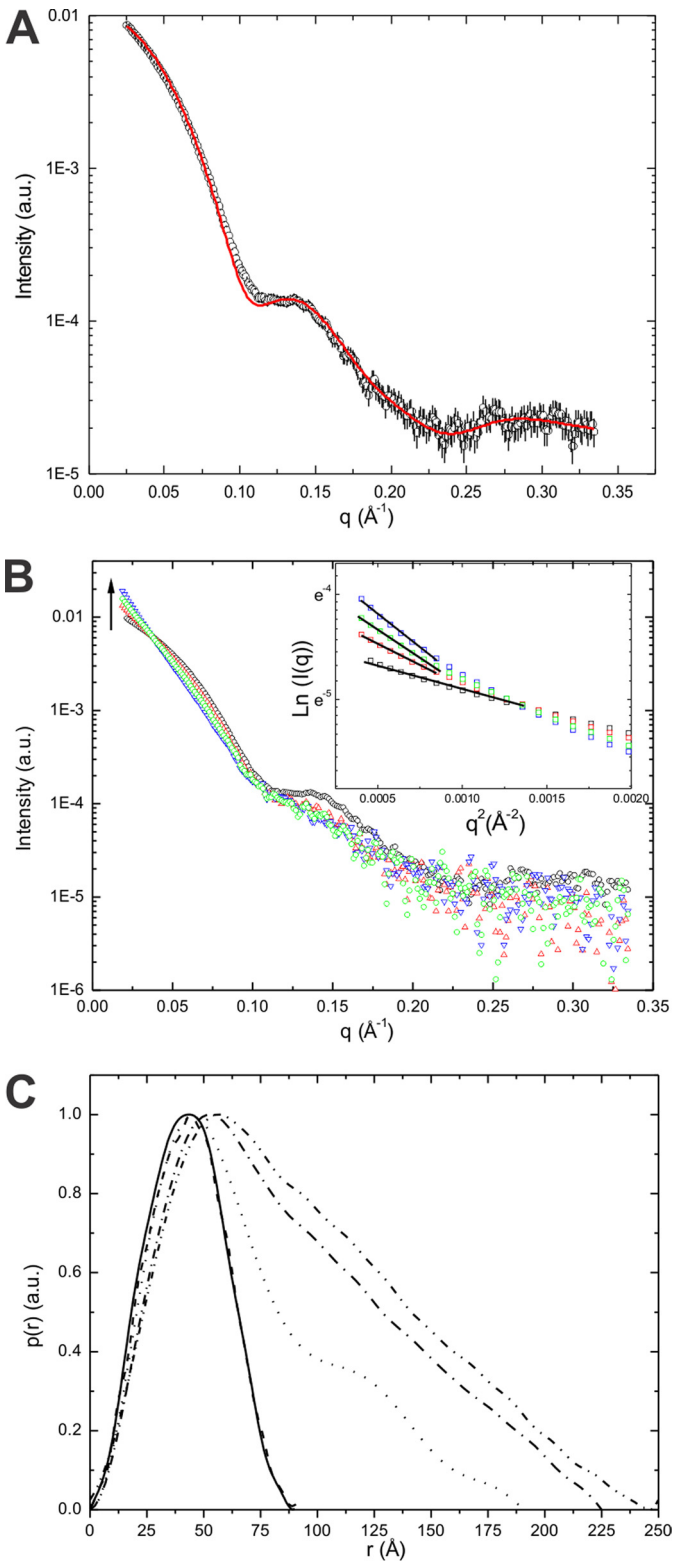

FIGURE 4. **SAXS curves and data analysis of GAPDH in the presence and in the absence of heparin.** *A*, correspondence between theoretical and experimental SAXS curves: the experimental values (*open squares*) were obtained by the scattering of 4 mg/ml GAPDH. The theoretical scattering curve (*red solid line*) calculated from the protein crystallographic structure (1J0X). *B*, SAXS data from 4 mg/ml GAPDH in solution in the absence (*black*) and in the presence of heparin at 2 min (*red*), 60 min (*green*), and 180 min (*blue*) of GAPDH-heparin interaction. The respective Guinier plots are displayed in the *inset*. *C*, corresponding pair distance distribution function, $p(r)$, calculated from the experimental scattering curve (*dashed line*) and from the homotetramer crystallographic structure (*solid line*), calculated by using the GNOM software (37); $p(r)$ functions in the presence of heparin after 2 min (*dotted line*), 60 min (*dashed-dotted line*), and 180 min (*dashed-double dotted line*) from the sample preparation.

appearance of the upturn in the $I(q)$ at low q values (Fig. 4*B*), demonstrate the formation of oligomers coexisting with native-like GAPDH already at 2 min of heparin addition in solution. Changes in GAPDH conformation were also noted by fluorescence (Fig. 1) and FTIR measurements (Fig. 3), which indicate an increase in the solvent accessibility to some hydrophobic region and some cross-β structure formation within less than 5 min of GAPDH-heparin interaction. We will return to this point later in the text. Of note, 1–3 h after the addition of heparin to the GADPH solution, the $p(r)$ functions (Fig. 4*C*) become typical for the scattering of elongated particles as rod-like cylinders or fibers (33). The maximum distance r of scattering centers inside the protein underwent a further increase (r increases to ~70 Å) relative to that observed over 2 min of the beginning of the GAPDH-heparin interaction (Fig. 4*C*). Such a value of r must be roughly related to the scattering particle cross-section (32). Note, however, that aggregates longer than D_{max} of ~300 Å cannot be detected by our experimental SAXS resolution. Therefore, SAXS and DLS results were combined to infer the time evolution of the aggregate dimensions as indicated below.

Size Distribution of the Oligomeric Species—The time evolution in the size distribution of GADPH incubated with heparin at 37 °C as studied through dynamic light scattering is shown in Fig. 5*A*. Prior to heparin addition, only a population with hydrodynamic diameter $D_H = 100 \pm 10$ Å was observed, which is compatible to the D_{max} value determined for the tetrameric GAPDH (Fig. 4*B*) in the absence of heparin. A new population with a mean value of $D_H = 400$ Å arose 15 min after the addition of heparin (Fig. 5*A*). This population continuously evolved to an average mean value of $D_H = 600$ and 1000 Å after 30 and 60 min, respectively. The self-assemblage of protein or heparin at 37 °C was discarded because no significant change in the scattering signal could be detected in DLS experiments (data not shown).

Glycolytic activity can be regarded as an indirect measure of the native tetrameric GAPDH population. After 1 h of preincubation with heparin, ~40% of the enzymatic activity was lost (Fig. 5*B*). These data reinforce the conclusion that two populations coexist under this condition, *i.e.* the enzymatically active tetrameric form with the inactive oligomeric species.

According to SAXS data (Fig. 4*B*) the heparin-induced GAPDH oligomers are rather anisometric. It is well known that for a nonspherical particle, such as a cylinder, the interpretation of the hydrodynamic radius (or diameter) is quite complex. Thus, it is possible to suppose that the proteins aggregates are arranged as thin rigid rods. For such cases, it is possible to write (38, 52) the following,

$$R_h \approx \frac{L}{2\ln(L/d)} \qquad \text{(Eq. 4)}$$

where R_h is the hydrodynamic radius obtained with DLS experiments, and L and d are the cylinder length and cross-section, respectively. It is also possible to rewrite the above equation as follows,

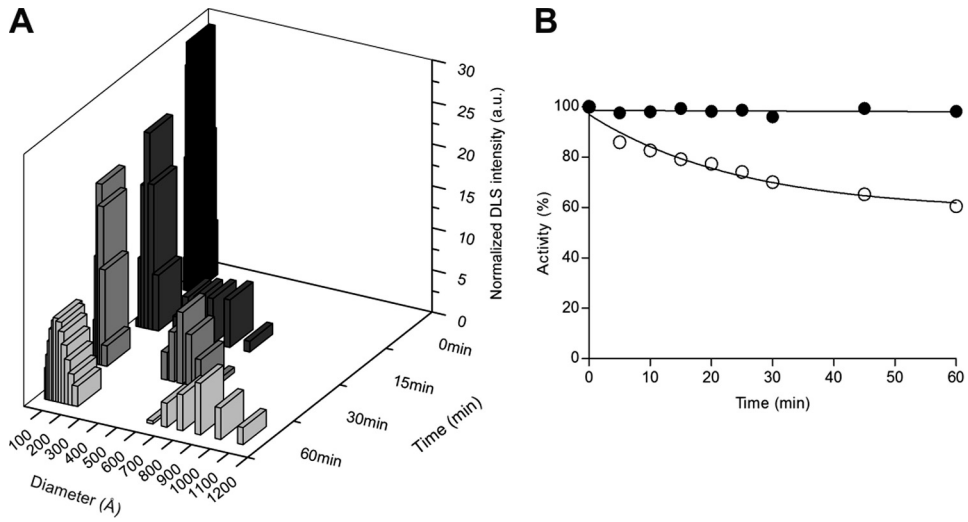

FIGURE 5. **DLS analysis and enzymatic activity of GAPDH in the presence and in the absence of heparin.** *A*, DLS measurements of GAPDH in solution along time in the presence of heparin. *B*, GAPDH (0.16 mg/ml) enzymatic activity in the absence (●) and presence of 75 μg/ml of heparin (○).

$$\frac{\ln(x)}{x} \approx \frac{d}{2R_h} \qquad \text{(Eq. 5)}$$

where $x = L/d$. Let us suppose that the cylinder cross-section is $d = \sim 70$ Å (from the inflection point of the $p(r)$ curve, as shown in Ref. 51), and $R_h = \sim 500$ Å (from the DLS experiments, where $D_h = \sim 1000$ Å). Thus, it is possible to calculate the heparin-induced GAPDH oligomer length L, which amounts to $L = \sim 4000$ Å.

Computational Prediction of Heparin-binding Site on GAPDH Structure—A global search for heparin-binding sites on GAPDH was conducted as detailed under "Experimental Procedures." The docking protocol was evaluated on a test set including protein-heparin complexes taken from the Brookhaven database. The observed values of RMSD for basic fibroblast growth factor (1.96 Å), acidic fibroblast growth factor (0.15 Å), and hepatocyte growth factor (1.63 Å) show small deviations from the crystallographic structure, reflecting the ability of the docking protocol to correctly localize heparin-binding sites. A global search for heparin-binding sites on the GAPDH surface using the same docking protocol resulted in the best docking position at the long linear groove formed by the interface between chains R and P close to the enzyme catalytic site. As seen in Fig. 6*A*, this groove has an overall positive electrostatic potential to readily accommodate the negatively charged ligand (53). Several positively charged amino acid residues are located in this region, allowing the formation of five hydrogen bonds between the oligosaccharide and the protein groove. Focused docking calculations were carried out on the lowest energy sites revealed by global hard-docking calculations to further optimize the protein-ligand interactions. Because of the large number of torsional degrees of freedoms in the heparin hexasaccharide, a fully flexible docking was not possible. Nevertheless, as shown by Khan *et al.* (54), heparin tends to adopt a semi-rigid and extended conformation for its optimal binding to proteins. In this way, torsion angles around the glycosidic bonds of the four central residues were kept fixed, whereas the others were allowed to rotate freely. Close-up views into the protein-ligand interactions, as well as a two-dimensional schematic representation are shown on Fig. 6 (*B* and *C*, respectively). Sulfate and carboxylate groups on heparin were found to form hydrogen bonds with Lys^{104}, Lys^{183}, and Lys^{191}. Viewed from the hexasaccharide reducing end, the sulfate group of the uronic acid 2 (sugar unit 2) was seen to directly interact with the amino group of Lys^{183}, whereas the carboxylate in the uronic 4 (sugar unit 4) and the sulfate group of the uronic acid 6 (sugar unit 6) both interact with Lys^{191}. Importantly, the sulfated glucosamine 5 (sugar 5) showed two points of interaction with Lys^{104} involving the *N*-sulfate and the hydroxyl group in its carbon 3 (C3).

GAGs Ability to Induce GAPDH Aggregation—To investigate whether the heparin-induced GAPDH aggregation is a general effect that could be attributable to other GAGs, the maximal ThT emission intensity over 60 min of incubation at 37 °C in the presence of HS, CS-A, CS-B, CS-C, and Dx was studied (Fig. 7*A*). The GAPDH aggregation obtained in the presence of HS showed a similar behavior than heparin but with less efficiency. On the contrary, in the presence of CS-A, CS-B, CS-C, and Dx, no changes in the fluorescence intensity were detected, even after a 10-fold increase in GAGs concentrations (data not shown). Conformational changes in GAPDH induced by the addition of different GAGs, as monitored by amide I′ band in the FTIR spectra, are shown on Fig. 6*B*. It seems to be clear that HS is the unique GAG tested that can mimic the heparin effect on GAPDH, because the spectra remain unchanged upon addition of CS-A, CS-B, CS-C, and Dx.

Heparin-induced GAPDH Aggregates Can Influence the AS Fibrillation Kinetics—It has been previously shown that AS aggregation is a nucleation-dependent process in which preformed aggregates can function as seeds increasing the rate of conversion from soluble specie into amyloid fibrils (55). The aggregation kinetics of AS in the absence as well as in the presence of different heparin-induced GAPDH aggregation states are shown in Fig. 8*A*. The addition of GAPDH amyloid fibrils, *i.e.* those obtained after 24 h of GAPDH:heparin incubation, are not able to produce significant changes on AS aggregation

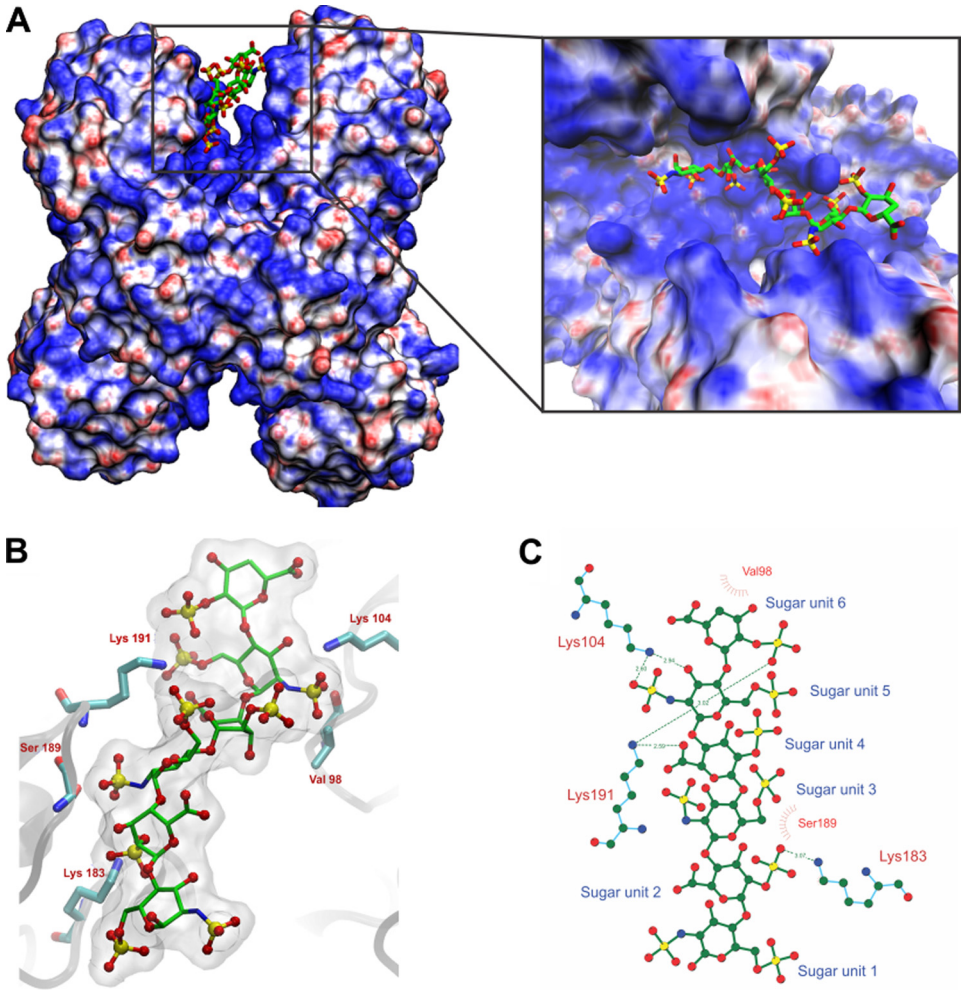

FIGURE 6. **Molecular docking simulation results of GAPDH and heparin.** *A*, front and close-up view of the protein-ligand complex. The licorice model is used to represent heparin hexasaccharide, whereas the electrostatic potential is mapped onto the solvent-accessible surface of the GAPDH; a *blue color* indicates a region of positive potential (+10 kT/e), *red* indicates a negative potential (−10 kT/e), and *white* indicates a neutral potential. *B*, binding mode of heparin to GAPDH with the protein shown in cartoon representation, with heparin and selected amino acids side chain in licorice representation. *C*, schematic representation of the interaction generated with Ligplot; the reducing end corresponds to the first sugar unit at the bottom of the hexasaccharide.

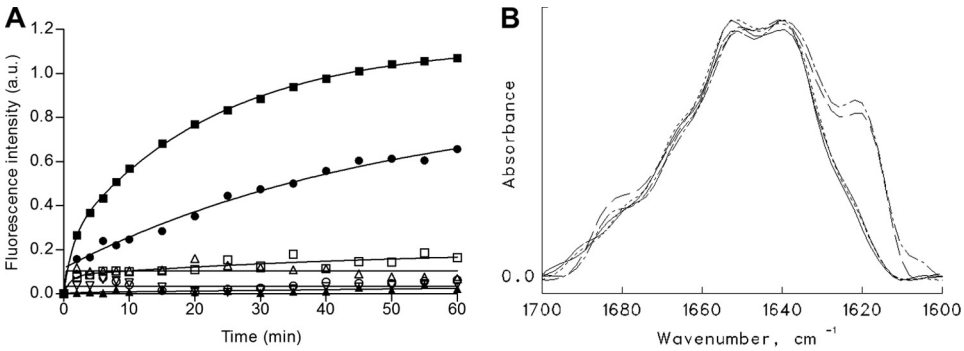

FIGURE 7. **Effect of different GAGs in GAPDH aggregation.** *A*, kinetics of GAG-induced GAPDH aggregation: ThT fluorescence emission of 0.16 mg/ml of GAPDH (▲) alone and in the presence of different GAGs: 75 μg/ml of heparin (■), HS (●), Dx (□), CS-B (△), and CS-C (△). *B*, FTIR deconvolved spectra in the amide I′ region of GAPDH alone (*solid line*) and in the presence CS-A (*pointed line*), CS-B (*dotted line*), CS-C (*solid line*), heparin (*dotted-dashed lines*), and HS (*dashed line*) after 60 min of incubation at 37 °C. The *line* represents the curve fit according to equation described under "Experimental Procedures."

kinetics. On the contrary, an exponential increase in ThT fluorescence intensity was observed upon the addition of heparin-induced GAPDH early oligomers (Fig. 8*A*). In the latter, the increase in ThT fluorescence emission could not be considered as direct effect of heparin on AS aggregation because the kinetics of the processes are not alike. In fact, after the first hour of AS:heparin incubation, ThT techniques were unable to detect any AS aggregation (9).

To probe the ability of heparin-induced GAPDH early oligomers to recruit AS, the fibrils obtained after 5 h of incubation were thoroughly washed to discard any adsorbed material and subjected to a disassembling protocol with urea 8 M as

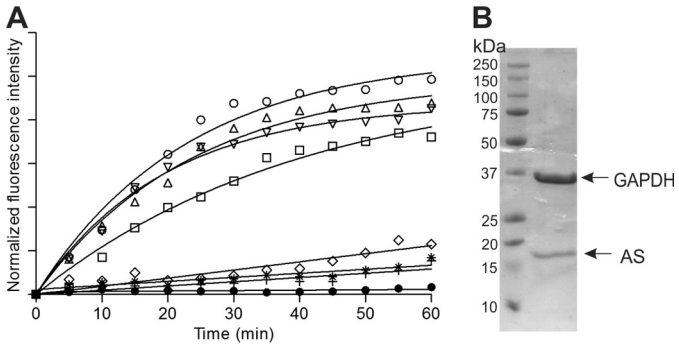

FIGURE 8. **Influence of GAPDH early oligomers in the AS aggregation kinetics.** *A*, aggregation kinetic of AS in the presence of heparin-induced GAPDH oligomers obtained after 5 min (○), 15 min (▽), 30 min (△), 60 min (□), and 24 h (*) of GAPDH-heparin interaction. Control experiments in the presence of GAPDH alone (+) and heparin (◇) are also depicted. The *line* represents the curve fit according to equation described under "Experimental Procedures." *B*, gel electrophoresis in SDS-PAGE of mixed fibrils. Protein was loaded as follows: *lane 1*, protein molecular weight marker; *lane 2*, washed fibrils. The positions of bands of GAPDH and AS are marked by *arrows*.

described under "Experimental Procedures." After the treatment, an SDS-PAGE analysis of the supernatant demonstrated the presence of two bands of ~14.5 and 36 kDa, attributable to AS and GAPDH monomers, respectively (Fig. 8*B*).

DISCUSSION

In the current study, we demonstrate the ability of heparin to trigger GAPDH aggregation into oligomers and amyloid fibrils by using different biophysical techniques. Oligomers were detected by DLS and SAXS, whereas their structures were inferred from infrared spectroscopy. The presence of amyloid fibrils was detected by fluorescence spectroscopy and microscopy. Analysis on DLS and SAXS showed the formation of oligomers during the first hour of heparin-GAPDH interaction, which was accompanied by a concomitant increase in ThT fluorescence. FTIR spectroscopy studies revealed the presence of cross-β structure in these early oligomers, which could account for the increment in ThT fluorescence emission. In this way we show that ThT, traditionally used as specific marker of the cross β-structure in amyloid fibrils (28), is also able to increase its intrinsic fluorescence upon binding to GAPDH oligomeric species as described on other systems (47).

ANS as well as tryptophan intrinsic fluorescence also reflect conformational changes occurring to GAPDH after heparin addition. Both techniques revealed the transition between four states, which we attribute to native, native-like, oligomeric, and fibrillar GAPDH. The results from other biophysical techniques, *i.e.* ThT fluorescence emission, FTIR, and SAXS, are also compatible with the existence of these states as discussed below.

FTIR spectroscopy provided complementary information allowing the quantification of conformational changes on GAPDH structure. Even though this technique cannot provide absolute values, the comparison between the amide I′ band components at different conditions is very useful to follow the conformational evolution of the system. Upon binding of heparin to GAPDH, the amide I′ band changes its contour mainly at the expense of the increment in the cross-β band, located at ~1618 cm^{-1}. Another conformational changes could be inferred such as the diminish in the 1623 cm^{-1}, attributable to a decrease in the intersubunits contacts according to (25). This hypothesis is also supported by shift in both ANS and Trp fluorescence emission already at 5 min of contact between heparin and GADPH, which could be attributed to the exposure to solvent of Trp^{193} and Trp^{310} located at the subunit interface in GAPDH native structure. In fact, inspection of the crystallographic structure evidences that the Trp^{193} is prone to increase its exposure to the solvent in the case that some slight rotation of the subunits takes place (supplemental Table S1). Such a hypothesis is consistent with SAXS results, where small changes in the protein dimensions were observed 5 min after the addition of heparin in GADPH solution. Moreover, FTIR data showed that the resultant species are conformationally slightly different from that of tetrameric species because cross β-structure is incremented at the expense of β-sheets and intersubunits contacts. ANS binding assays reveal an increase in the hydrophobic surface exposed to the solvent with time, which is probably more "sticky" and prone to aggregate according to fluorescence, infrared, and DLS studies. It is important to note that according to our results, the aggregation pathway for GAPDH does not pass through a partial unfolding state because the α-helix and the overall β-structures contents remain almost unaltered, as we confirmed by CD (supplemental Fig. S2). The differences between the FTIR data could be explained because FTIR resolves with better accuracy the β-sheet composition (56).

SAXS is an adequate technique to investigate proteins at low resolution. Moreover, this technique allows evaluating proteins in solution at different times. The SAXS data presented herein provide a structural description of the heparin-induced GAPDH aggregation process from the enzymatically active tetrameric enzyme to the formation of early oligomers. Under our experimental conditions and in the absence of heparin, GAPDH remains in a stable tetrameric form with a R_g value of 32.9 Å. Upon 1 h of heparin interaction, GAPDH aggregates are clearly revealed by the increase in the forward scattering intensity. The early oligomerization states can be described as short rod-like cylinders. The quite linear behavior of the $p(r)$ function for the $r > 70$ Å range suggests that the heparin-induced GAPDH aggregates elongates in one dimension (33).

The DLS data can give a picture of the population size of each aggregation state at different times. It is important to note that the tetrameric population is still present after 1 h of GAPDH: heparin incubation together with the oligomeric component. In fact, the population centered around D_H = 120 Å was quite broad, indicating the presence of a heterogeneous mixture of small oligomers together with the tetrameric enzyme. Taken together, the SAXS and DLS results support the conclusion that after 1 h of GAPDH-heparin interaction, rod-like aggregates as long as 4000 Å are present together with tetrameric and small aggregate species in solution. The residual enzymatic activity still detectable after 1 h of incubation of GAPDH in the presence of heparin also supports the hypothesis that a part of the tetrameric species is still present.

Overall, a model for heparin-induced GAPDH aggregation pathway can be proposed as follows: native → native-like → oligomers → fibril, which is in line with the previously described model for Sso AcP (57) and SOD1 (58). The results are also compatible with a transition involving tetramer dissociation, as seen on

transthyretin (59) and membrane-induced GAPDH (25) amyloidogenic processes, although such a monomeric state could not be isolated under our experimental conditions.

Even though the effect of GAGs on protein fibrillation has been reported for many proteins involved in human diseases, this model does not seem to be of general character because the GAGs chemical structure, particularly concerning the sulfate group position, strongly influence the GAPDH amyloidogenic abilities. In fact CS-C, which is characterized by the presence of sulfate groups in position 6 of the GalNAc residues, did not have any effect on GAPDH fibril formation, but it was effective in stimulating aggregation of Aβ peptide (11). Accordingly, CS-A and CS-B are also efficient to induce the AS fibrillation (9). The relevance of the GAGs sulfate group density on the polysaccharides ability to promote the amyloidogenic process was previously reported for transthyretin (60, 61). However, on GAPDH aggregation, the position of the sulfate groups on the polymeric sugar chain seems to be more important than their density because only heparin and HS, but not CS, contain *N*-sulfated residues and 3-free hydroxyl groups in the glucosamine unit. Moreover, the 2-*O*-sulfation in the uronic unit residue of heparin and HS is absent in CS-A and CS-B. The importance of these particular functional groups in heparin and HS is here shown by their availabilities to interact with Lys^{104}, Lys^{183}, and Lys^{191} on GAPDH. Interestingly, *N*-sulfation and 2-*O*-sulfation contents are higher in heparin than in HS, which might explain the higher effect observed with the high sulfated polysaccharide. It is also important to consider that although the docking calculations were performed with hexasaccharide species of heparin to reduce the simulation time, the polysaccharide commonly contains more than 50 sugar units. This implies that the groove formed between the other two subunits in GAPDH could also bind to the polysaccharide chain.

In this work, the ability of heparin-induced GAPDH oligomers to promote AS aggregation kinetics is demonstrated. The structural similitude between heparin with HS-induced GAPDH oligomers suggests that the latter could exhibit the same recruiting effect. Considering the toxicity of AS soluble oligomeric species (62, 63), therapeutic strategies aimed to reduce fibril formation (*e.g.* stabilization of the folded state by small molecules) might paradoxically enhance neurotoxicity. Therefore, the elimination of soluble oligomers, either by preventing their formation or by promoting their incorporation into fibrils, can be expected to reduce AS cytotoxicity in cells. We are currently working in this area. The ability of heparin-induced GAPDH oligomers to promote AS fibril formation may now be used as a basis for new *in vivo* studies investigating novel therapeutic strategies.

Acknowledgments—We are grateful to Dr. Ricardo Farías for valuable discussions and to Dr. Francesco Spinozzi and Dr. Paolo Mariani, who provided SASMOL software. We acknowledge the National Laboratory of Synchrotron Light (Campinas, SP, Brazil) for the use of SAXS beam line facilities and CNPq.

REFERENCES

1. Tong, J., Wong, H., Guttman, M., Ang, L. C., Forno, L. S., Shimadzu, M., Rajput, A. H., Muenter, M. D., Kish, S. J., Hornykiewicz, O., and Furukawa, Y. (2010) Brain α-synuclein accumulation in multiple system atrophy, Parkinson's disease and progressive supranuclear palsy. A comparative investigation. *Brain* **133,** 172–188
2. Spillantini, M. G., Crowther, R. A., Jakes, R., Hasegawa, M., and Goedert, M. (1998) α-Synuclein in filamentous inclusions of Lewy bodies from Parkinson's disease and dementia with Lewy bodies. *Proc. Natl. Acad. Sci. U.S.A.* **95,** 6469–6473
3. Nussbaum, R. L., and Ellis, C. E. (2003) Alzheimer's disease and Parkinson's disease. *N. Engl. J. Med.* **348,** 1356–1364
4. Anderson, J. P., Walker, D. E., Goldstein, J. M., de Laat, R., Banducci, K., Caccavello, R. J., Barbour, R., Huang, J., Kling, K., Lee, M., Diep, L., Keim, P. S., Shen, X., Chataway, T., Schlossmacher, M. G., Seubert, P., Schenk, D., Sinha, S., Gai, W. P., and Chilcote, T. J. (2006) Phosphorylation of Ser-129 is the dominant pathological modification of α-synuclein in familial and sporadic Lewy body disease. *J. Biol. Chem.* **281,** 29739–29752
5. Spillantini, M. G., Schmidt, M. L., Lee, V. M., Trojanowski, J. Q., Jakes, R., and Goedert, M. (1997) α-Synuclein in Lewy bodies. *Nature* **388,** 839–840
6. Tatton, W. G., Chalmers-Redman, R. M., Elstner, M., Leesch, W., Jagodzinski, F. B., Stupak, D. P., Sugrue, M. M., and Tatton, N. A. (2000) Glyceraldehyde-3-phosphate dehydrogenase in neurodegeneration and apoptosis signaling. *J. Neural. Transm.* (suppl.) **60,** 77–100
7. Liu, C., Fei, E., Jia, N., Wang, H., Tao, R., Iwata, A., Nukina, N., Zhou, J., and Wang, G. (2007) Assembly of lysine 63-linked ubiquitin conjugates by phosphorylated α-synuclein implies Lewy body biogenesis. *J. Biol. Chem.* **282,** 14558–14566
8. Perry, G., Richey, P., Siedlak, S. L., Galloway, P., Kawai, M., and Cras, P. (1992) Basic fibroblast growth factor binds to filamentous inclusions of neurodegenerative diseases. *Brain Res.* **579,** 350–352
9. Cohlberg, J. A., Li, J., Uversky, V. N., and Fink, A. L. (2002) Heparin and other glycosaminoglycans stimulate the formation of amyloid fibrils from α-synuclein *in vitro*. *Biochemistry* **41,** 1502–1511
10. Ancsin, J. B. (2003) Amyloidogenesis: historical and modern observations point to heparan sulfate proteoglycans as a major culprit. *Amyloid* **10,** 67–79
11. Castillo, G. M., Lukito, W., Wight, T. N., and Snow, A. D. (1999) The sulfate moieties of glycosaminoglycans are critical for the enhancement of β-amyloid protein fibril formation. *J. Neurochem.* **72,** 1681–1687
12. Cotman, S. L., Halfter, W., and Cole, G. J. (2000) Agrin binds to β-amyloid (Aβ), accelerates Aβ fibril formation, and is localized to Aβ deposits in Alzheimer's disease brain. *Mol. Cell Neurosci.* **15,** 183–198
13. Valle-Delgado, J. J., Alfonso-Prieto, M., de Groot, N. S., Ventura, S., Samitier, J., Rovira, C., and Fernàndez-Busquets, X. (2010) Modulation of Aβ42 fibrillogenesis by glycosaminoglycan structure. *FASEB J.* **24,** 4250–4261
14. Papy-Garcia, D., Christophe, M., Huynh, M. B., Fernando, S., Ludmilla, S., Sepulveda-Diaz, J. E., and Raisman-Vozari, R. (2011) Glycosaminoglycans, protein aggregation and neurodegeneration. *Curr. Protein Pept. Sci.* **12,** 258–268
15. Jeffery, C. J. (2009) Moonlighting proteins. An update. *Mol. Biosyst.* **5,** 345–350
16. Huberts, D. H., and van der Klei, I. J. (2010) Moonlighting proteins. An intriguing mode of multitasking. *Biochim. Biophys. Acta* **1803,** 520–525
17. Sirover, M. A. (1999) New insights into an old protein. The functional diversity of mammalian glyceraldehyde-3-phosphate dehydrogenase. *Biochim. Biophys. Acta* **1432,** 159–184
18. Sugahara, T., Shirahata, S., Sasaki, T., and Murakami, H. (1995) The mode of actions of glyceraldehyde-3-phosphate dehydrogenase identified as an immunoglobulin production stimulating factor. *FEBS Lett.* **368,** 92–96
19. Yamaji, R., Chatani, E., Harada, N., Sugimoto, K., Inui, H., and Nakano, Y. (2005) Glyceraldehyde-3-phosphate dehydrogenase in the extracellular space inhibits cell spreading. *Biochim. Biophys. Acta* **1726,** 261–271
20. Tatton, N. A. (2000) Increased caspase 3 and Bax immunoreactivity accompany nuclear GAPDH translocation and neuronal apoptosis in Parkinson's disease. *Exp. Neurol.* **166,** 29–43
21. Tsuchiya, K., Tajima, H., Kuwae, T., Takeshima, T., Nakano, T., Tanaka, M., Sunaga, K., Fukuhara, Y., Nakashima, K., Ohama, E., Mochizuki, H.,

Mizuno, Y., Katsube, N., and Ishitani, R. (2005) Pro-apoptotic protein glyceraldehyde-3-phosphate dehydrogenase promotes the formation of Lewy body-like inclusions. *Eur. J. Neurosci.* **21,** 317–326
22. Kragten, E., Lalande, I., Zimmermann, K., Roggo, S., Schindler, P., Muller, D., van Oostrum, J., Waldmeier, P., and Furst, P. (1998) Glyceraldehyde-3-phosphate dehydrogenase, the putative target of the antiapoptotic compounds CGP 3466 and R-(−)-deprenyl. *J. Biol. Chem.* **273,** 5821–5828
23. Maruyama, W., Akao, Y., Youdim, M. B., Davis, B. A., and Naoi, M. (2001) Transfection-enforced Bcl-2 overexpression and an anti-Parkinson drug, rasagiline, prevent nuclear accumulation of glyceraldehyde-3-phosphate dehydrogenase induced by an endogenous dopaminergic neurotoxin, *N*-methyl(*R*)salsolinol. *J. Neurochem.* **78,** 727–735
24. Zhao, H., Tuominen, E. K., and Kinnunen, P. K. (2004) Formation of amyloid fibers triggered by phosphatidylserine-containing membranes. *Biochemistry* **43,** 10302–10307
25. Cortez, L. M., Avila, C. L., Bugeau, C. M., Farías, R. N., Morero, R. D., and Chehín, R. N. (2010) Glyceraldehyde-3-phosphate dehydrogenase tetramer dissociation and amyloid fibril formation induced by negatively charged membranes. *FEBS Lett.* **584,** 625–630
26. Hoyer, W., Antony, T., Cherny, D., Heim, G., Jovin, T. M., and Subramaniam, V. (2002) Dependence of α-synuclein aggregate morphology on solution conditions. *J. Mol. Biol.* **322,** 383–393
27. Corbier, C., Clermont, S., Billard, P., Skarzynski, T., Branlant, C., Wonacott, A., and Branlant, G. (1990) Probing the coenzyme specificity of glyceraldehyde-3-phosphate dehydrogenases by site-directed mutagenesis. *Biochemistry* **29,** 7101–7106
28. LeVine, H., 3rd (1999) Quantification of β-sheet amyloid fibril structures with thioflavin T. *Methods Enzymol.* **309,** 274–284
29. Arrondo, J. L., Muga, A., Castresana, J., and Goñi, F. M. (1993) Quantitative studies of the structure of proteins in solution by Fourier-transform infrared spectroscopy. *Prog. Biophys. Mol. Biol.* **59,** 23–56
30. Arrondo, J. L., Castresana, J., Valpuesta, J. M., and Goñi, F. M. (1994) Structure and thermal denaturation of crystalline and noncrystalline cytochrome oxidase as studied by infrared spectroscopy. *Biochemistry* **33,** 11650–11655
31. Bañuelos, S., Arrondo, J. L., Goñi, F. M., and Pifat, G. (1995) Surface-core relationships in human low density lipoprotein as studied by infrared spectroscopy. *J. Biol. Chem.* **270,** 9192–9196
32. Cowan-Jacob, S. W., Kaufmann, M., Anselmo, A. N., Stark, W., and Grütter, M. G. (2003) Structure of rabbit-muscle glyceraldehyde-3-phosphate dehydrogenase. *Acta Crystallogr. D Biol. Crystallogr.* **59,** 2218–2227
33. Glatter, O., and Kratky, O. (1982) Small-angle X-ray Scattering. Academic Press, New York
34. Ortore, M. G., Spinozzi, F., Mariani, P., Paciaroni, A., Barbosa, L. R., Amenitsch, H., Steinhart, M., Ollivier, J., and Russo, D. (2009) Combining structure and dynamics: non-denaturing high-pressure effect on lysozyme in solution. *J. R Soc. Interface* **6,** (Suppl. 5) S619–S634
35. Barbosa, L. R., Ortore, M. G., Spinozzi, F., Mariani, P., Bernstorff, S., and Itri, R. (2010) The importance of protein-protein interactions on the pH-induced conformational changes of bovine serum albumin. A small-angle X-ray scattering study. *Biophys. J.* **98,** 147–157
36. Guinier, A., and Fournet, G. (1955) *Small angle scattering of X-rays*, Wiley, New York
37. Svergun, D. I. (1992) Determination of the regularization parameter in indirect-transform methods using perceptual criteria. *J. Appl. Crystallogr.* **25,** 495–503
38. Krysmann, M. J., Castelletto, V., McKendrick, J. E., Clifton, L. A., Hamley, W. I., Harris, P. J., and King, S. M. (2008) Self-assembly of peptide nanotubes in an organic solvent. *Langmuir* **24,** 8158–8162
39. Zhang, J., and Snyder, S. H. (1992) Nitric oxide stimulates auto-ADP-ribosylation of glyceraldehyde-3-phosphate dehydrogenase. *Proc. Natl. Acad. Sci. U.S.A.* **89,** 9382–9385
40. Bitomsky, W., and Wade, R. C. (1999) Docking of glycosaminoglycans to heparin-binding proteins: Validation for aFGF, bFGF, and antithrombin and application to IL-8. *J. Am. Chem. Soc.* **121,** 3004–3013
41. Humphrey, W., Dalke, A., and Schulten, K. (1996) VMD: visual molecular dynamics. *J. Mol. Graph.* **14,** 33–38, 27–38
42. Baker, N. A., Sept, D., Joseph, S., Holst, M. J., and McCammon, J. A. (2001) Electrostatics of nanosystems. Application to microtubules and the ribosome. *Proc. Natl. Acad. Sci. U.S.A.* **98,** 10037–10041
43. Wallace, A. C., Laskowski, R. A., and Thornton, J. M. (1995) LIGPLOT. A program to generate schematic diagrams of protein-ligand interactions. *Protein Eng.* **8,** 127–134
44. Lowry, O. H., Rosebrough, N. J., Farr, A. L., and Randall, R. J. (1951) Protein measurement with the Folin phenol reagent. *J. Biol. Chem.* **193,** 265–275
45. Dische, Z., and Borenfreund, E. (1950) A spectrophotometric method for the microdetermination of hexosamines. *J. Biol. Chem.* **184,** 517–522
46. Weber, K., and Osborn, M. (1969) The reliability of molecular weight determinations by dodecyl sulfate-polyacrylamide gel electrophoresis. *J. Biol. Chem.* **244,** 4406–4412
47. Carrotta, R., Bauer, R., Waninge, R., and Rischel, C. (2001) Conformational characterization of oligomeric intermediates and aggregates in β-lactoglobulin heat aggregation. *Protein Sci.* **10,** 1312–1318
48. Eakin, C. M., Attenello, F. J., Morgan, C. J., and Miranker, A. D. (2004) Oligomeric assembly of native-like precursors precedes amyloid formation by β-2 microglobulin. *Biochemistry* **43,** 7808–7815
49. Durrieu, C., Bernier-Valentin, F., and Rousset, B. (1987) Microtubules bind glyceraldehyde-3-phosphate dehydrogenase and modulate its enzyme activity and quaternary structure. *Arch. Biochem. Biophys.* **252,** 32–40
50. Arrondo, J. L., Young, N. M., and Mantsch, H. H. (1988) The solution structure of concanavalin A probed by FT-IR spectroscopy. *Biochim. Biophys. Acta* **952,** 261–268
51. Barbosa, L. R., Itri, R., Caetano, W., Neto Dde, S., and Tabak, M. (2008) Self-assembling of phenothiazine compounds investigated by small-angle x-ray scattering and electron paramagnetic resonance spectroscopy. *J. Phys. Chem. B* **112,** 4261–4269
52. Riseman, J., and Kirkwood, J. G. (1950) The Intrinsic viscosity, translational and rotatory diffusion constants of rod-like macromolecules in solution. *J. Chem. Physics* **18,** 512–516
53. Avila, C. L., de Arcuri, B. F., Gonzalez-Nilo, F., De Las Rivas, J., Chehín, R., and Morero, R. (2008) Role of electrostatics on membrane binding, aggregation and destabilization induced by NAD(P)H dehydrogenases. Implication in membrane fusion. *Biophys. Chem.* **137,** 126–132
54. Khan, S., Gor, J., Mulloy, B., and Perkins, S. J. (2010) Semi-rigid solution structures of heparin by constrained x-ray scattering modelling. New insight into heparin-protein complexes. *J. Mol. Biol.* **395,** 504–521
55. Wood, S. J., Wypych, J., Steavenson, S., Louis, J. C., Citron, M., and Biere, A. L. (1999) α-Synuclein fibrillogenesis is nucleation-dependent. Implications for the pathogenesis of Parkinson's disease. *J. Biol. Chem.* **274,** 19509–19512
56. Calero, M., and Gasset, M. (2005) Fourier transform infrared and circular dichroism spectroscopies for amyloid studies. *Methods Mol. Biol.* **299,** 129–151
57. Bemporad, F., and Chiti, F. (2009) "Native-like aggregation" of the acylphosphatase from *Sulfolobus solfataricus* and its biological implications. *FEBS Lett.* **583,** 2630–2638
58. Elam, J. S., Taylor, A. B., Strange, R., Antonyuk, S., Doucette, P. A., Rodriguez, J. A., Hasnain, S. S., Hayward, L. J., Valentine, J. S., Yeates, T. O., and Hart, P. J. (2003) Amyloid-like filaments and water-filled nanotubes formed by SOD1 mutant proteins linked to familial ALS. *Nat. Struct. Biol.* **10,** 461–467
59. Hurshman, A. R., White, J. T., Powers, E. T., and Kelly, J. W. (2004) Transthyretin aggregation under partially denaturing conditions is a downhill polymerization. *Biochemistry* **43,** 7365–7381
60. Bourgault, S., Solomon, J. P., Reixach, N., and Kelly, J. W. (2011) Sulfated glycosaminoglycans accelerate transthyretin amyloidogenesis by quaternary structural conversion. *Biochemistry* **50,** 1001–1015
61. McLaurin, J., Franklin, T., Zhang, X., Deng, J., and Fraser, P. E. (1999) Interactions of Alzheimer amyloid-β peptides with glycosaminoglycans effects on fibril nucleation and growth. *Eur. J. Biochem.* **266,** 1101–1110
62. Haass, C., and Selkoe, D. J. (2007) Soluble protein oligomers in neurodegeneration. Lessons from the Alzheimer's amyloid β-peptide. *Nat. Rev. Mol. Cell Biol.* **8,** 101–112
63. Caughey, B., and Lansbury, P. T. (2003) Protofibrils, pores, fibrils, and neurodegeneration. Separating the responsible protein aggregates from the innocent bystanders. *Annu. Rev. Neurosci.* **26,** 267–298